Available online at www.sciencedirect.com
SCIENCE DIRECT®
International Journal of Thermal Sciences 43 (2004) 489–498
International Journal of Thermal Sciences
www.elsevier.com/locate/ijts

Mixed convection flow in a narrow vertical duct filled with a porous medium

I. Pop [a,*], D.A.S. Rees [b], C. Egbers [c]

[a] *Faculty of Mathematics, University of Cluj, R-3400 Cluj, CP 253, Romania*
[b] *Department of Mechanical Engineering, University of Bath, Claverton Down, Bath, BA2 7AY, UK*
[c] *Department of Aerodynamics and Fluidmechanics (LAS), Brandenburg Technical University (BTU), 03044 Cottbus, Germany*

Received 5 June 2003; accepted 29 September 2003

Abstract

This paper presents a theoretical study of mixed convection flow in a vertical duct filled with a fluid-saturated porous medium under the assumption that ε, the ratio of the duct width to the heated length, is small, i.e., that the duct is narrow. It is assumed that a fully developed flow has already been set up in the duct before localised heating on one wall causes the flow to be changed by the action of buoyancy forces, as measured by the mixed convection parameter, λ. An analytical solution is derived for the case when both the Péclet number, *Pe*, and λ are of $O(1)$. It is found that reversed flow appears at leading order when $\lambda > 2$. This is confirmed by numerical integrations of the governing equations, for $P = \varepsilon Pe = 100$ and a range of values of λ, where $\varepsilon \to 0$ and $Pe = O(\varepsilon^{-1})$. The limiting cases of $P \ll 1$ and $P \gg 1$ (boundary layer) with λ variable and $\lambda \to \infty$ (free convection limit) are also studied. The numerical results show very good agreement with the analytical and asymptotic solutions.

1. Introduction

Heat transfer induced by buoyancy effects in fluid-saturated porous media has received considerable attention over the last several decades because of numerous applications in geophysics and energy-related engineering problems. Such applications include heat exchangers, porous insulations, solar power collectors, heat storage beds, nuclear waste disposals, energy efficient drying processes, enhanced recovery of petroleum resources, underground spread of pollutants and building structure insulation and food processing, to name but a few. All these applications have led to the large number of publications in this area of heat transfer. A detailed review of the subject, including exhaustive lists of references, can be found in the books by Ingham and Pop [1], Nield and Bejan [2], Vafai [3], and Pop and Ingham [4].

In the context of thermal insulation applications, one can identify a large class of convection problems consisting of heat transfer in a differentially heated porous cavity. Analytical work includes numerical solutions, boundary layer solutions, integral analyses, and series solutions. A detailed review of this topic, was recently performed by Vafai and Hadim [5], and Lai [6].

Recent technological implications have given rise to increased interest in mixed convection problems in vertical channels, pipes and annuli because of their applications in nuclear reactors, heat exchangers, electronic system cooling, etc. The fully-developed and parallel flow assumptions are often made and analytical solutions become available to facilitate the analysis of heat transfer characteristics. From these studies it became clear that there were two major influences on the heat transfer, namely the geometrical configuration and the developed fluid flow. This interaction between the heat transfer and the fluid flow of a viscous (non-porous) fluid has been first considered by Mahmood and Merkin [7]. They studied the mixed connection flow in a vertical duct under the assumption that the ratio of the duct width to the length over which the wall is heated is small. In addition, it was assumed that a fully developed Poiseuille flow has already been set up in the duct before heat from the wall causes this to be changed by the action of the buoyancy forces.

A review of the open literature reveals, however, that there has been less attention paid to mixed convection in a vertical duct filled with a porous medium, see Lai [6].

* Corresponding author.
E-mail address: popi@math.ubbcluj.ro (I. Pop).

1290-0729/$ – see front matter
doi:10.1016/j.ijthermalsci.2003.09.004

Nomenclature

g	gravitational acceleration	$m\cdot s^{-1}$
h	width of the duct	m
K	permeability	m^2
l	length of the heated section of the duct wall	m
p^*	pressure	$kg\cdot m^{-1}\cdot s^{-2}$
P	modified Péclet number for a porous medium	
Pe	Péclet number for a porous medium	
q_0, q_1	non-dimensional heat fluxes on the walls	
Q	prescribed flow rate	$m^2\cdot s^{-1}$
R	modified Rayleigh number for a porous medium	
Ra	Rayleigh number for a porous medium	
T	fluid temperature	K
T_0	ambient temperature	K
u, v	non-dimensional velocities in the x and y directions, respectively	
x, y	non-dimensional Cartesian coordinates	

Greek letters

α_m	effective thermal diffusivity	$m^2\cdot s^{-1}$
β	thermal expansion coefficient	K^{-1}
ΔT	applied temperature difference	K
ε	ratio of the duct width to heated length	
λ	mixed convection parameter	
μ	dynamic viscosity	$kg\cdot m^{-1}\cdot s^{-1}$
ν	kinematic viscosity	$m^2\cdot s^{-1}$
θ	non-dimensional temperature	
ψ	non-dimensional streamfunction	

Subscript

w	evaluated at the wall

Superscripts

$*$	dimensional variables
$'$	differentiation with respect to x

Hadim [8] carried out a numerical study of buoyancy-assisted mixed convection in an isothermally heated vertical channel filled with a fluid-saturated porous medium. He employed the Darcy–Brinkman–Forchheimer model and presented results in terms of the modified Grashof number, *Gr*, Darcy number, *Da*, Reynolds number, *Re*, inertial coefficient, *F*, and the Prandtl number, *Pr*. These results show that the effects of varying the Grashof and Reynolds numbers for a given Darcy number only affect the region close to the entrance; and in the fully developed region, forced convection dominates the overall heat transfer. In the Darcy flow regime, the heat transfer rate is governed by the single mixed convection parameter Gr/Re. The Nusselt number increases with Gr/Re in the inlet region but is independent of this parameter in the fully developed region.

It is not possible to compare the present results with those of Hadim [8] since the temperature profiles considered there are different from those in the present paper, and, further, Hadim's work lies squarely within the elliptic regime where upstream influence is significant, whereas the present work is within the parabolic regime due to the narrowness of the gap compared with the streamwise distance over which the boundary temperature profile varies.

Mixed convection in a vertical porous channel subject to asymmetric wall heating conditions has been studied by Hadim and Chen [9]. Two heating conditions have been considered: uniform wall temperature and uniform wall heat flux, respectively. Their results show that the heat transfer enhancement in the mixed convection regime is more pronounced for the heating condition by uniform wall temperature than by uniform wall heat flux.

Lai et al. [10] have carried out a numerical study to examine the effects of forced flow on free convection induced by a finite heat source on an otherwise adiabatic vertical wall of a two-dimensional wall channel. The channel was considered to be isothermally cooled. In the absence of a forced flow, it is expected that a recirculatory flow will be induced by an isolated heat source. The buoyancy-induced flow pattern is significantly modified when an external pressure gradient causes upflow. When the forced flow is weak, buoyancy effects dominate the velocity field generally. However, the acceleration caused by buoyancy forces deflects the main flow toward the heat source, causing a recirculation zone at the cold wall side. An increase in the externally induced velocity, or Péclet number, moves the convective cell upward. This delays the separation of the main flow from the cold wall. When the Péclet number is large, the enhanced thermal convection in the upward direction weakens the opposing buoyant effects on the cold wall. As a result, the strength of the secondary flow decreases substantially.

The purpose of the present paper is therefore to examine the mixed convection flow in a vertical duct filled with a porous medium assuming that a temperature difference is applied on one wall of the duct, while the other wall is maintained at a constant ambient temperature. It is also assumed that a fully developed flow has already been set up in the duct before heat from the wall causes this to be changed by the action of the buoyancy forces, as measured by the mixed convection parameter λ. Under these assumptions, we shall study the case of a narrow duct, that is, where the ratio of the duct width to the length over which the wall is heated, ε, is small, a case considered by Mahmood and Merkin [7] for a clear fluid narrow duct. We consider first the case when the Péclet number, *Pe*, and the mixed convection parameter λ are of $O(1)$. Here the problem of solving the basic equations for $\varepsilon \ll 1$ can be reduced to a simple analytical calculation in powers of ε. This solution

shows regions of reversed flow for both heated ($\lambda > 0$) and cooled ($\lambda < 0$) walls in line with the numerical study made by Lai et al. [10]. However, the analytical solution obtained for $Pe = O(1)$ breaks down when Pe is of $O(\varepsilon^{-1})$ and the governing equations, written in terms of λ and the modified Péclet number, $P = \varepsilon Pe$, are solved numerically using the Keller-box method for a range of values of λ and P. Analytical solutions are also presented for cases where $P \ll 1$ with λ fixed. Finally, numerical solutions for the boundary layer case, $P \gg 1$, are presented for a choice of values of λ and cases where P is fixed and $\lambda \gg 1$ (the free convection limit).

2. Basic equations

Consider the problem of steady mixed convection flow in a vertical duct filled with a fluid-saturated porous medium. We assume that the convecting fluid and the porous medium are everywhere in local thermodynamic equilibrium, that the temperature of the fluid is everywhere below boiling point, that Darcy's law and the Boussinesq approximation hold, that the properties of the fluid and the porous medium are constant except for the density in the Darcy's law, that the porous medium is homogeneous and isotropic, and that boundary, thermal dispersion and viscous dissipation effects are neglected. Under these assumptions, the governing differential equations are, see Nield and Bejan [2],

$$\frac{\partial u^*}{\partial x^*} + \frac{\partial v^*}{\partial y^*} = 0 \tag{1}$$

$$\frac{\partial u^*}{\partial y^*} - \frac{\partial v^*}{\partial x^*} = \frac{gK\beta}{\nu}\frac{\partial T}{\partial y^*} \tag{2}$$

$$u^*\frac{\partial T}{\partial x^*} + v^*\frac{\partial T}{\partial y^*} = \alpha_m\left(\frac{\partial^2 T}{\partial x^{*2}} + \frac{\partial^2 T}{\partial y^{*2}}\right) \tag{3}$$

where u^* and v^* are the velocity components in the x^* and y^* directions, respectively, T is the fluid temperature, g is the acceleration due to gravity, K is the permeability of the porous medium, β is the coefficient of thermal expansion, ν is the kinematic viscosity, α_m is the effective thermal diffusivity, and x^*, y^* are the Cartesian coordinates as shown in Fig. 1. We assume that the boundary conditions to be applied are

$$\begin{aligned} &v^* = 0 \quad \text{on } y^* = 0 \text{ and } y^* = h \\ &T = T_0 \quad \text{on } y^* = h \\ &T = T_0 + \Delta T\theta_w(x) \quad \text{on } y^* = 0,\ |x^*| < l \end{aligned} \tag{4}$$

together with the constant flux condition that

$$\int_0^h u^*\,\mathrm{d}y^* = Q \tag{5}$$

where h is the width of the duct, T_0 is the ambient temperature, l is the streamwise extent of the applied

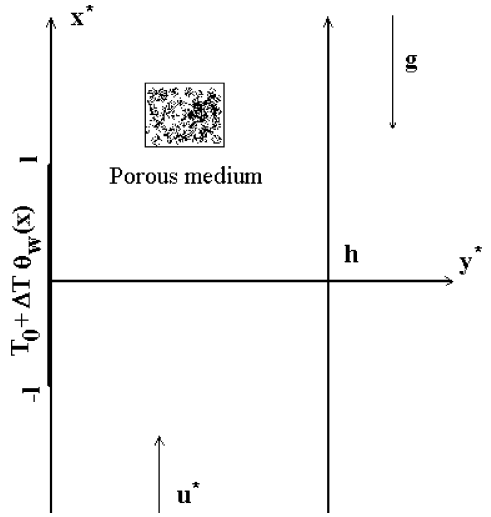

Fig. 1. Physical model and coordinate system.

temperature difference ΔT, Q is the (prescribed) flow rate and $\theta_w(x)$ is the (non-dimensional) temperature distribution on the duct wall $y^* = 0$ with $\theta_w(x)$ localized to a region of streamwise extent of $O(1)$, i.e., we take $\theta_w(x) = 0$ for $|x| > 1$. Consequently, well upstream (i.e., as $x^* \to -\infty$) the flow will be unaffected by the heat supplied from the wall $y^* = 0$ and will be given by

$$u^* = -\frac{K}{\mu}\frac{\partial p^*}{\partial x^*} = \text{const.}, \qquad v^* = 0, \qquad T = T_0 \tag{6}$$

To make Eqs. (1)–(3) non-dimensional, we define the following variables:

$$\begin{aligned} &x = x^*/l, \qquad y = y^*/h, \qquad u = (h/Q)u^* \\ &v = (l/Q)v^*, \qquad T - T_0 = \Delta T\theta \end{aligned} \tag{7}$$

so that we get

$$\frac{\partial u}{\partial x} + \frac{\partial v}{\partial y} = 0 \tag{8}$$

$$\frac{\partial u}{\partial y} - \varepsilon^2\frac{\partial v}{\partial x} = \lambda\frac{\partial \theta}{\partial y} \tag{9}$$

$$\frac{\partial^2\theta}{\partial y^2} + \varepsilon^2\frac{\partial^2\theta}{\partial x^2} = \varepsilon Pe\left(u\frac{\partial\theta}{\partial x} + v\frac{\partial\theta}{\partial y}\right) \tag{10}$$

where ε is the ratio of duct width to heated length, Pe is the Péclet number for a porous medium and λ is the buoyancy or mixed convection parameter, which are defined as

$$\varepsilon = h/l, \qquad Pe = Q/\alpha_m, \qquad \lambda = Ra/Pe \tag{11}$$

with $Ra = gK\beta\Delta Th/\nu\alpha_m$ being the Rayleigh number for a porous medium.

The boundary conditions (4) together with the flux condition (5) become

$$\begin{aligned} &v = 0 \quad \text{on } y = 0 \text{ and } y = 1 \\ &\theta = \theta_w(x) \quad \text{on } y = 0,\ |x| < 1, \qquad \theta = 0 \quad \text{on } y = 1 \end{aligned} \tag{12}$$

and

$$\int_0^1 u \, \mathrm{d}y = 1 \tag{13}$$

Further, we introduce the streamfunction ψ defined in the usual way as

$$u = \frac{\partial \psi}{\partial y}, \qquad v = -\frac{\partial \psi}{\partial x} \tag{14}$$

so that Eqs. (9) and (10) can be written as

$$\frac{\partial^2 \psi}{\partial y^2} + \varepsilon^2 \frac{\partial^2 \psi}{\partial x^2} = \lambda \frac{\partial \theta}{\partial y} \tag{15}$$

$$\frac{\partial^2 \theta}{\partial y^2} + \varepsilon^2 \frac{\partial^2 \theta}{\partial x^2} = \varepsilon Pe \left(\frac{\partial \psi}{\partial y} \frac{\partial \theta}{\partial x} - \frac{\partial \psi}{\partial x} \frac{\partial \theta}{\partial y} \right) \tag{16}$$

subject to

$$\begin{aligned} &\psi = 0 \quad \text{on } y = 0, \qquad \psi = 1 \quad \text{on } y = 1 \\ &\theta = \theta_w(x) \quad \text{on } y = 0,\ |x| < 1, \qquad \theta = 0 \quad \text{on } y = 1 \end{aligned} \tag{17}$$

where the boundary condition $\psi = 1$ on $y = 1$ results in from (13) and (14). We shall now consider different cases depending on the parameters ε, Pe and λ. Attention is restricted to positive values of λ since the symmetry of the problem is such that the same equations and boundary conditions are obtained when making the transformation $\lambda \to -\lambda$, $\psi \to -\psi$ and $x \to -x$. Negative values of λ correspond to a cooled strip.

3. Analysis

3.1. Narrow duct flow, $\varepsilon \ll 1$, Pe and λ of $O(1)$

In this case, we look for a solution of Eqs. (15) and (16) of the form

$$\begin{aligned} &\psi = \psi_0 + \varepsilon \psi_1 + \varepsilon^2 \psi_2 + \cdots \\ &\theta = \theta_0 + \varepsilon \theta_1 + \varepsilon^2 \theta_2 + \cdots \end{aligned} \tag{18}$$

Substituting these series into Eqs. (15) and (16), and applying the boundary condition (17), we get, after some algebra,

$$\begin{aligned} \theta_0 &= (1 - y)\theta_w(x) \\ \psi_0 &= y + \frac{1}{2}\lambda \theta_w \left(y - y^2 \right) \\ \theta_1 &= Pe \theta_w' \left[-\frac{1}{3}y + \frac{1}{2}y^2 - \frac{1}{6}y^3 \right. \\ &\qquad \left. + \lambda \theta_w \left(-\frac{1}{8}y + \frac{1}{4}y^2 - \frac{1}{6}y^3 + \frac{1}{24}y^4 \right) \right] \\ \psi_1 &= \lambda Pe \theta_w' \left[\frac{1}{24}y - \frac{1}{6}y^2 + \frac{1}{6}y^3 - \frac{1}{24}y^4 \right. \\ &\qquad \left. + \lambda \theta_w \left(\frac{1}{80}y - \frac{1}{16}y^2 + \frac{1}{12}y^3 - \frac{1}{24}y^4 + \frac{1}{120}y^5 \right) \right] \end{aligned} \tag{19}$$

where primes denote differentiation with respect to x.

It is seen from (19) that, in order to determine the flow and heat transfer characteristics, we have to specify a functional form for $\theta_w(x)$. Following Mahmood and Merkin [7], we take

$$\theta_w(x) = \begin{cases} \cos^2\left(\dfrac{\pi x}{2} \right) & \text{for } |x| < 1 \\ 0 & \text{for } |x| > 1 \end{cases} \tag{20}$$

as this function and its first derivative are continuous at $|x| = 1$.

3.2. Narrow gap approximation, $\varepsilon \to 0$, and Pe of $O(\varepsilon^{-1})$

3.2.1. Numerical solution

It is seen from Eq. (16) that the series solution (18) breaks down when Pe is of $O(\varepsilon^{-1})$, i.e., when the convective terms in this equation become important to leading order. In this case we put

$$P = \varepsilon Pe \tag{21}$$

where P, a modified Péclet number for a porous medium, is a constant of $O(1)$. Eqs. (15) and (16) then become

$$\frac{\partial^2 \psi}{\partial y^2} = \lambda \frac{\partial \theta}{\partial y} \tag{22}$$

$$\frac{\partial^2 \theta}{\partial y^2} = P \left(\frac{\partial \psi}{\partial y} \frac{\partial \theta}{\partial x} - \frac{\partial \psi}{\partial x} \frac{\partial \theta}{\partial y} \right) \tag{23}$$

and are subjected to the boundary conditions (17) with $\theta_w(x)$ given by Eq. (20). In addition, we have to specify the starting conditions of Eqs. (22) and (23) since these equations are parabolic. These starting conditions can be obtained from the first equations of (6) as

$$u = 1, \qquad \theta = 0 \quad \text{for } x = -1 \tag{24}$$

or

$$\psi = y, \qquad \theta = 0 \quad \text{for } x = -1 \tag{25}$$

where we put const $= Q/l$. In fact, the condition (25) should be applied as $x \to -\infty$, but the parabolic nature of Eqs. (22) and (23) ensures that we can replace the condition $x \to -\infty$ by $x = -1$.

The physical quantity of importance for this problem is the heat flux on the walls which is given by

$$q_0 = -\left(\frac{\partial \theta}{\partial y} \right)_{y=0}, \qquad q_1 = -\left(\frac{\partial \theta}{\partial y} \right)_{y=1} \tag{26}$$

3.2.2. Analytical solution for $P \ll 1$

The solution of Eqs. (15) and (16) subject to the boundary conditions, (17), for $P \ll 1$ and λ fixed can be obtained from Eqs. (18) and (19) as

$$\psi = y + \frac{1}{2}\lambda \theta_w \left(y - y^2 \right)$$

$$+\lambda P\theta_w'\left[\left(\frac{1}{24}y-\frac{1}{6}y^2+\frac{1}{6}y^3-\frac{1}{24}y^4\right)+\lambda\theta_w\left(\frac{1}{80}y-\frac{1}{16}y^2+\frac{1}{12}y^3-\frac{1}{24}y^4+\frac{1}{120}y^5\right)\right]+\cdots \tag{27}$$

$$\theta=\theta_w(1-y)+P\theta_w'\left[-\frac{1}{3}y+\frac{1}{2}y^2-\frac{1}{6}y^3+\lambda\theta_w\left(-\frac{1}{8}y+\frac{1}{4}y^2-\frac{1}{6}y^3+\frac{1}{24}y^4\right)\right]+\cdots$$

Thus, we have

$$\begin{aligned} q_0&=\theta_w(x)+P\theta_w'\left(\frac{1}{3}+\frac{1}{8}\lambda\theta_w\right)+\cdots\\ q_1&=\theta_w(x)-\frac{1}{6}P\theta_w'\left(1+\frac{1}{4}\lambda\theta_w\right)+\cdots \end{aligned} \tag{28}$$

3.2.3. The free convection limit, $\lambda\to\infty$

In this case, we take

$$\psi=\lambda\phi(x,y) \tag{29}$$

and keep the modified Rayleigh number $R=\lambda P=\varepsilon Ra$ fixed as $\lambda\to\infty$. Eqs. (22) and (23) then become

$$\frac{\partial^2\phi}{\partial y^2}=\frac{\partial\theta}{\partial y} \tag{30}$$

$$\frac{\partial^2\theta}{\partial y^2}=R\left(\frac{\partial\phi}{\partial y}\frac{\partial\theta}{\partial x}-\frac{\partial\phi}{\partial x}\frac{\partial\theta}{\partial y}\right) \tag{31}$$

with the boundary conditions

$$\begin{aligned} &\phi=0, \qquad \theta=\theta_w(x) \quad \text{on } y=0\\ &\phi=\lambda^{-1}, \qquad \theta=0 \quad \text{on } y=1 \end{aligned} \tag{32}$$

and

$$\phi=\lambda^{-1}y, \qquad \theta=0 \quad \text{as } x\to-\infty \tag{33}$$

Further, we assume that $R\approx\lambda^{-1}$ and take $R_0=\lambda R$. The boundary conditions (32) suggest the following expansion for $\lambda\gg1$:

$$\begin{aligned} \phi&=\phi_0+\lambda^{-1}\phi_1+\lambda^{-2}\phi_2+\cdots\\ \theta&=\theta_0+\lambda^{-1}\theta_1+\lambda^{-2}\theta_2+\cdots \end{aligned} \tag{34}$$

where the functions ϕ_i and θ_i, $i=0,1,2,\ldots$ can be obtained in analytical form. After some algebra, we get

$$\psi=\frac{1}{2}\theta_w\left(y-y^2\right)+\frac{1}{2}R\theta_w\theta_w'\left(\frac{1}{40}y-\frac{1}{8}y^2+\frac{1}{6}y^3-\frac{1}{12}y^4+\frac{1}{60}y^5\right)+\lambda^{-1}y+\cdots \tag{35}$$

$$\theta=\theta_w(1-y)+\frac{1}{2}R\theta_w\theta_w'\left(-\frac{1}{4}y+\frac{1}{2}y^2-\frac{1}{3}y^3+\frac{1}{12}y^4\right)+\lambda^{-1}R\theta_w'\left(-\frac{1}{3}y+\frac{1}{2}y^2-\frac{1}{6}y^3\right)+\frac{1}{2}R^2\theta_w\theta_w'\left(\frac{1}{10080}y+\frac{1}{80}y^2-\frac{1}{40}y^3+\frac{1}{96}y^4+\frac{1}{120}y^5-\frac{1}{120}y^6+\frac{1}{5040}y^7\right)+\frac{1}{8}R^2\theta_w\left(\theta_w\theta_w'\right)'\left(\frac{23}{2520}y-\frac{1}{15}y^3+\frac{1}{8}y^4-\frac{1}{10}y^5+\frac{7}{180}y^6-\frac{2}{315}y^7\right)+\cdots \tag{36}$$

Thus, we have

$$q_0=\theta_w(x)+\frac{R}{8}\theta_w\theta_w'+\frac{R\theta_w'}{3\lambda}-\frac{R^2}{20160}\theta_w\left(\theta_w'\right)^2-\frac{23R^2}{20160}\theta_w\left(\theta_w\theta_w'\right)'+\cdots \tag{37}$$

$$q_1=\theta_w(x)-\frac{R}{24}\theta_w\theta_w'-\frac{R\theta_w'}{6\lambda}+\frac{3R^2}{2240}\theta_w\theta_w'+\frac{R^2}{4032}\theta_w\left(\theta_w\theta_w'\right)'+\cdots \tag{38}$$

3.2.4. Numerical solutions for $P\gg1$

An asymptotic balance of terms as $P\to\infty$ in Eqs. (22) and (23) suggests the scalings,

$$\begin{aligned} &x=X, \qquad y=P^{-1/2}Y\\ &\psi=P^{-1/2}\Psi(X,Y), \qquad \theta=\Theta(X,Y) \end{aligned} \tag{39}$$

Thus, we get the following boundary layer equations:

$$\frac{\partial^2\Psi}{\partial Y^2}=\lambda\frac{\partial\Theta}{\partial Y} \tag{40}$$

$$\frac{\partial^2\Theta}{\partial Y^2}=\frac{\partial\Psi}{\partial Y}\frac{\partial\Theta}{\partial X}-\frac{\partial\Psi}{\partial X}\frac{\partial\Theta}{\partial Y} \tag{41}$$

subject to the boundary conditions,

$$\begin{aligned} &\Psi=0, \qquad \Theta=\theta_w(X) \quad \text{on } Y=0, \quad \text{and}\\ &\frac{\partial\Psi}{\partial Y}\to1, \qquad \Theta\to0 \quad \text{as } Y\to\infty \end{aligned} \tag{42}$$

The condition for large values of Y allow the streamfunction and temperature fields to return to the state of uniform velocity and zero temperature which exists outside the boundary layer.

4. Results and discussion

Eqs. (22), (23), (30), (31) and (40), (41) have been solved numerically for various values of the parameters P and λ using the Keller-box method. This method is described in detail in the book by Cebeci and Bradshaw [11]. It is a parabolic solver, and its usual implementation uses multi-dimensional Newton–Raphson iteration to solve the discretised equations (written in first order form) at each successive streamwise position. The grid sizes used in the streamwise and normal directions are $\delta x=0.005$ and $\delta y=0.01$, respectively, for computations corresponding to

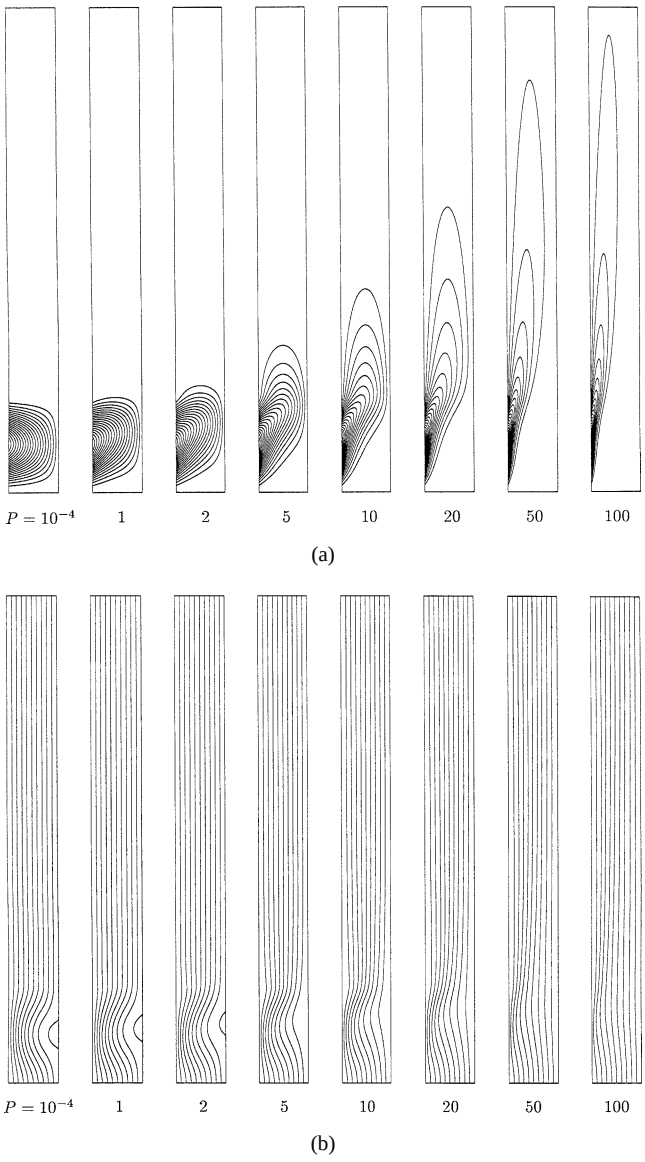

Fig. 2. (a) Isotherms and (b) streamlines for $\lambda = 2.5$ and for $P = 10^{-4}$ (top frame), 1, 2, 5, 10, 20, 50, and 100 (bottom frame). 19 equally spaced isotherms are drawn at an interval of 0.05 and 9 equally spaced streamlines at an interval of 0.1.

$P = O(1)$. Some representative results for the flow and heat transfer characteristics are shown in Figs. 2–12.

Fig. 2(a) and (b) show the computed isotherms and streamlines, respectively, for the case $\lambda = 2.5$ for a variety of values of P. When P is very small we recover the solution corresponding to the leading term in the expansion (18) for θ where the conduction takes place solely across the layer with neither conduction nor advection up the layer. As the value of P increases, forced convective effects become stronger and the effect of the localised heating spreads increasingly far downstream. Once the Péclet number is as large as 100 a distinct boundary layer has formed, which only just impinges on the unheated wall within the computational domain used.

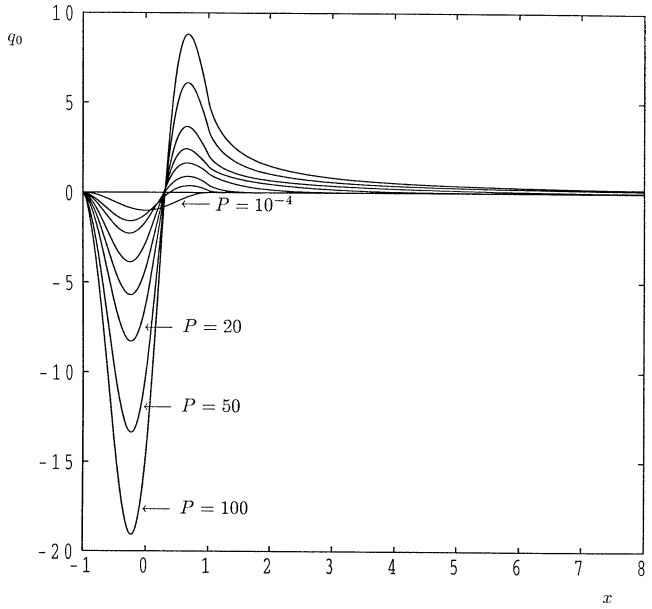

Fig. 3. Variation with x of the heat transfer at the left wall for $\lambda = 2.5$ and for $P = 10^{-4}$, 1, 2, 5, 10, 20, 50, and 100.

On differentiating the analytical solution given by ψ_0 in Eq. (19), we see that reversed flow should appear in the leading order solution once $\lambda > 2$, and, for $\lambda = 2.5$, a region of reversed flow may be expected to be well-established, as may be seen in Fig. 2(b). However, for the cases shown, the recirculation is quite weak, and is sufficiently so that it was possible to integrate through these regions without the Keller-box method losing its numerical stability. Equivalent solutions for $\lambda = 3$ and $P = 10^{-4}$ cannot be obtained since the recirculation is too strong. Again, as P increases, forced convective effects increases and the streamlines appear to become more uniform, with a slight deviation towards the heated strip.

These results are summarised in Figs. 3 and 4 which show the rates of heat transfer on the $y = 0$ and $y = 1$ walls, respectively. On the heated surface, $y = 0$, the temperature gradient remains negative when P is small reflecting the fact that the temperature field is passive with respect to x. At higher values of P the heat transfer is multiply-signed—once the fluid near the heated strip has been warmed it then travels downstream and encounters a relatively cold surface, and therefore the sign of the rate of heat transfer changes. We see in Fig. 3 that the position where the heat transfer takes its most negative value is upstream of where the surface attains it maximum value; this is due to the fact that the temperature field develops from the leading edge of the heated strip and the region of non-zero temperature thickens. Once the fluid is downstream of the heated strip there is gradual recovery towards the zero heat transfer situation where the fluid in the channel returns to a uniform temperature.

In Fig. 4 the heat transfer on the uncooled wall, $y = 1$, is shown. This figure illustrates how effective the flow is in delaying the spread of the thermal field to the $y = 1$ surface. The position of maximum absolute heat transfer

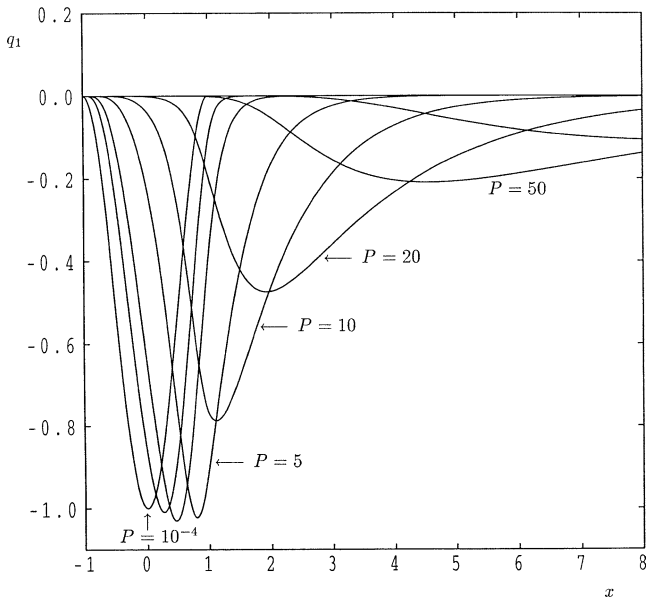

Fig. 4. Variation with x of the heat transfer at the right wall for $\lambda = 2.5$ and for $P = 10^{-4}$, 1, 2, 5, 10, 20, 50, and 100.

travels downstream as P increases. Moreover, the largest absolute heat transfer also decreases with increasing P simply because the fluid has travelled further along a cold channel before the peak is encountered.

Figs. 5–8 are concerned with the effects of varying λ for one value of P, namely, $P = 100$. Fig. 5 shows the isotherms and streamlines for these cases. Since $P = 100$ the flows already show a distinct boundary layer character. The primary effect of increasing λ is to increase the free convective effects. This is seen in two different ways in Fig. 5(a): first, the thermal field spreads further downstream and second, the thermal boundary layer becomes thinner near the heated strip. Both of these effects may be attributed to greater streamwise velocities induced within the cavity. The corresponding streamlines in Fig. 5(b) show a much greater distortion than those shown in Fig. 2(b). When λ is relatively large the flowfield near the heated strip is very similar qualitatively to that corresponding to an isolated heated surface in an unbounded fluid; a distinct entrainment into the developing thermal boundary layer is evident.

In each numerical simulation we calculated the minimum streamwise velocity, $\min_y \partial\psi/\partial y$, as a function of x. In Fig. 6 we display these values for the case $P = 100$. The position of minimum streamwise velocity, which always occurs on the cold surface, moves forward as λ increases. However, when $\lambda = 12.23856$, the minimum streamwise velocity is zero, and therefore, at greater values of λ there is recirculation.

The local heat transfers from each surface are shown in Figs. 7 and 8, where it is important to note the different scalings on both axes. The position of the maximum absolute rate of heat transfer on the hot surface at $y = 0$ is affected only very slightly by variations in λ, since the flow may be regarded as being within the boundary layer regime

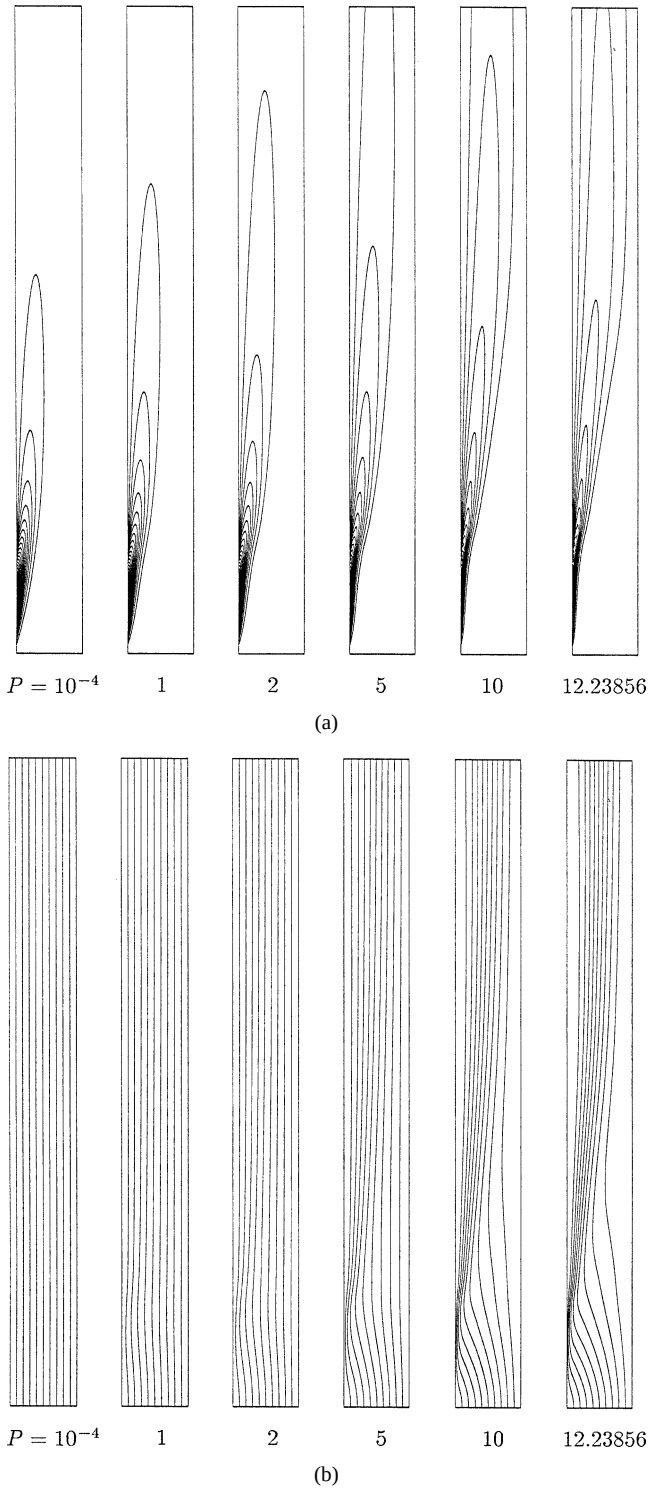

Fig. 5. (a) Isotherms and (b) streamlines for $P = 100$ and $\lambda = 10^{-4}$ (top frame), 1, 2, 5, 10, and 12.23856. 19 equally spaced isotherms are drawn at an interval of 0.05 and 9 equally spaced streamlines at an interval of 0.1.

due to the size of P, and therefore changes in λ serve only to modify the thickness of the boundary layer. On the other hand, at the cold surface, the position when the magnitude of the heat transfer is maximised moves further downstream as λ increases. This is consistent with

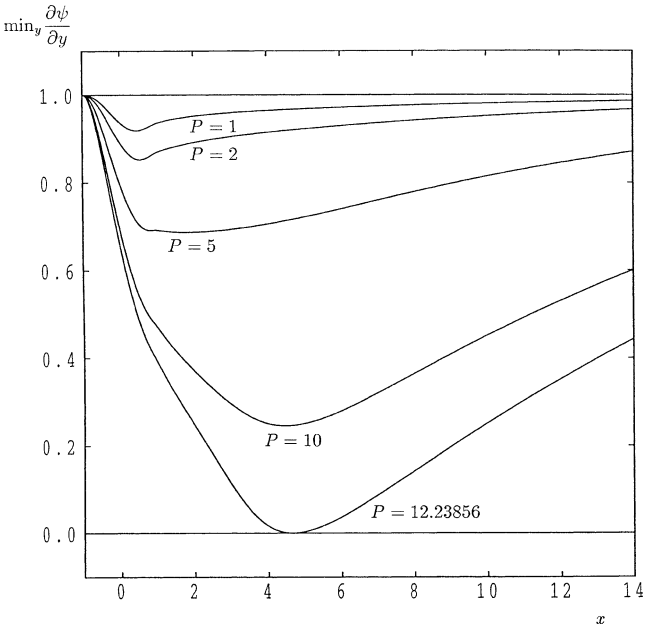

Fig. 6. Variation with x of the minimum streamwise velocity for $P = 100$ and $\lambda = 10^{-4}$ (top frame), 1, 2, 5, 10, and 12.23856 (bottom frame).

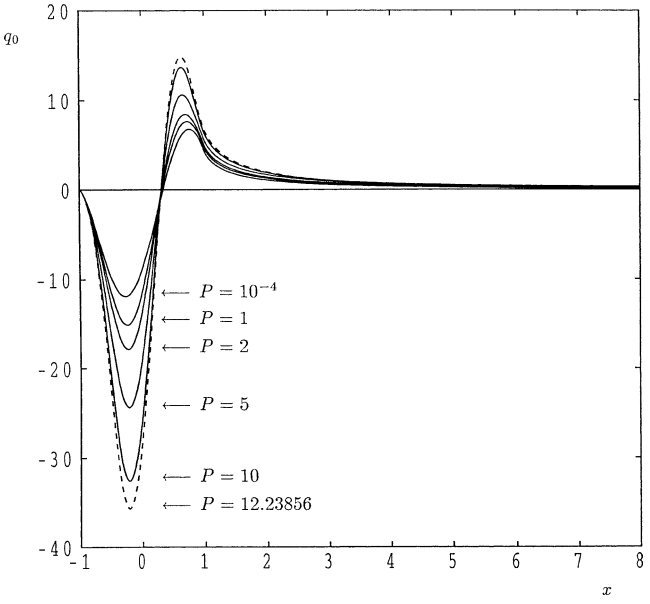

Fig. 7. Variation with x of the heat transfer at the left wall for $P = 100$ and $\lambda = 10^{-4}$, 1, 2, 5, 10, and 12.23856.

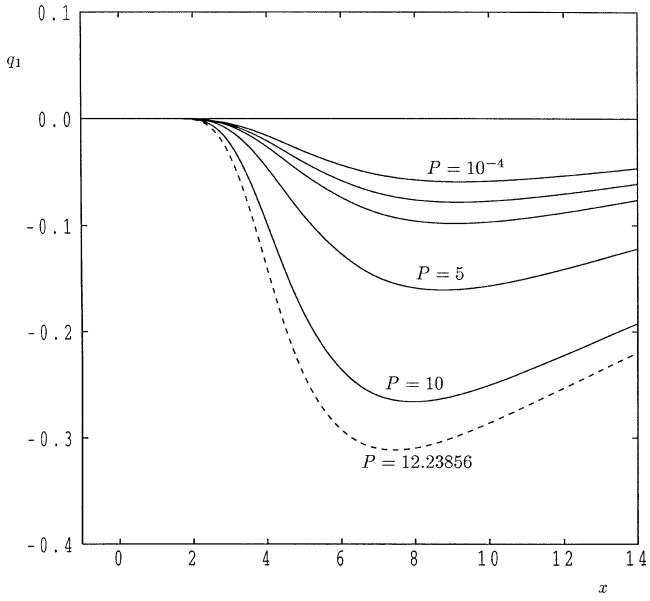

Fig. 8. Variation with x of the heat transfer at the right wall for $P = 100$ and $\lambda = 10^{-4}$, 1, 2, 5, 10, and 12.23856.

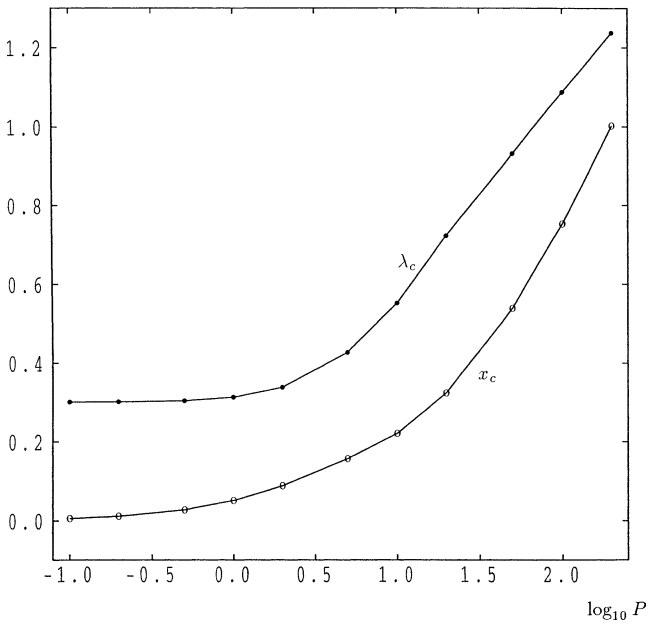

Fig. 9. Variation with $\log_{10} P$ of the value of λ above which separation occurs and the corresponding value of x at which separation first arises.

the increasing vigour of the flow rendering cross-stream conduction less effective.

In the two main cases considered so far, the results we were able to obtain are, in general, subject to the restriction that there must be no recirculation. For example, for $P = 100$, we able to compute a flow for which $\lambda = 12.3$, but not for $\lambda = 12.4$ for which recirculation is stronger. Therefore we have computed, for the sake of reference, the value of λ above which recirculation occurs as a function of P, and the corresponding value of x at which the minimum streamwise velocity is zero. These values are shown in Fig. 9. When P is small the critical value of λ is close to 2, which is consistent with the analysis of Section 3.1 and the comment in the third paragraph of this section. Numerically we find that $\lambda_c = 2 + O(P^2)$ when $P \ll 1$. On the other hand, for $P \gg 1$, then $\lambda_c \sim 1.22P^{1/2}$. The corresponding critical values of x are $x_c \sim 0.13P$ for $P \ll 1$ and $x_c \sim 0.05P$ for $P \gg 1$. The coefficients quoted here are necessarily inaccurate because they are not only subject to the discretisation errors inherent in the Keller-box method, but are also subject to interpolation errors due to

the fact that they are obtained from discrete solutions of a marching method.

Fig. 10 compares the heat transfer on the wall $y = 0$ which is obtained by solving Eqs. (22) and (23) for $\lambda = 1$ and $P = 50, 100$, with that obtained from the $P \to \infty$ boundary layer equations, (40) and (41). It is found that $P^{-1/2}\partial\theta/\partial y|_{y=0}$ matches very well with $\partial\Theta/\partial Y|_{Y=0}$. In fact, Fig. 11 shows that the asymptotic rate of heat transfer, $\partial\Theta/\partial Y|_{Y=0}$, retains the same shape as those shown in Figs. 3 and 7.

Finally, Fig. 12 shows the isotherms and streamlines in the $P \to \infty$ limit for various values of λ. All the streamlines are depicted at intervals of 1 in order to facilitate comparison between the cases. It is seen that the shapes of the thermal boundary layer match well with the $P = O(1)$ cases (see Figs. 2(a) and 12(a)). However, when λ is large, there is a thinning of the thermal boundary layer. The streamlines

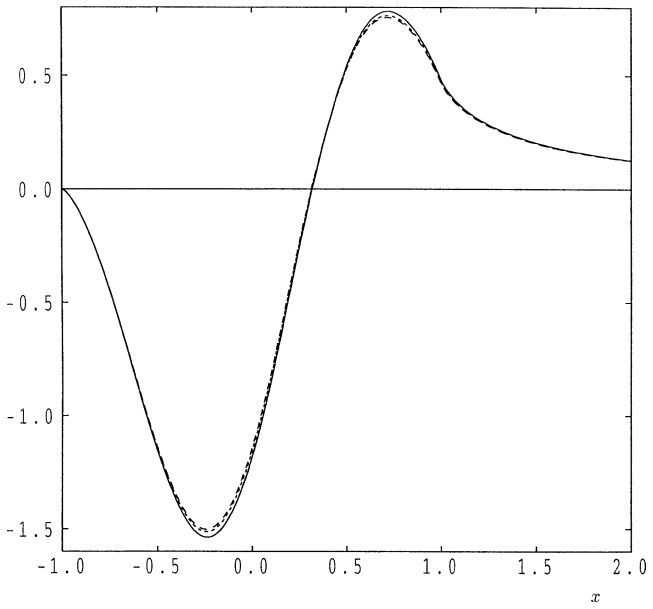

Fig. 10. Variation with x (or X) of the left wall rate of heat transfer for $\lambda = 1$. The continuous line corresponds to $\partial\Theta/\partial Y|_{Y=0}$ from the large-P asymptotic theory, while the short and long dashed lines correspond to $P^{-1/2}\partial\theta/\partial y|_{y=0}$, for $P = 100$ and $P = 50$, respectively.

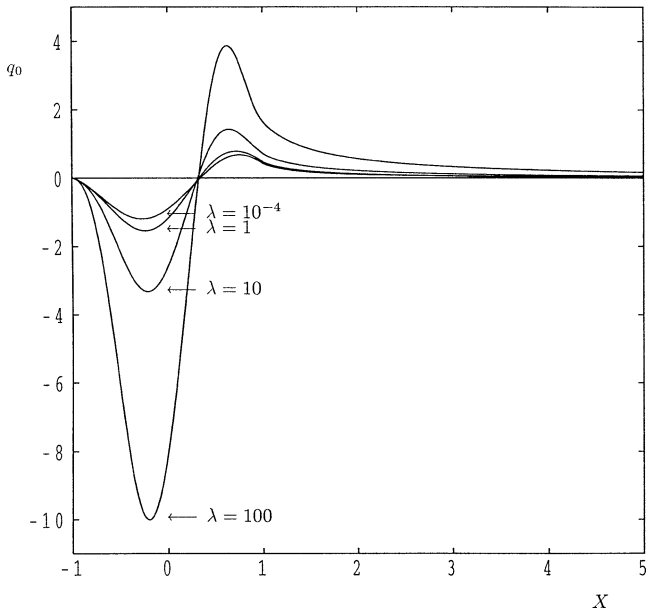

Fig. 11. Variation with X of the heat transfer at the left wall, $Y = 0$, for $P \to \infty$, the boundary layer limit, for $\lambda = 10^{-4}$, 1, 10, and 100.

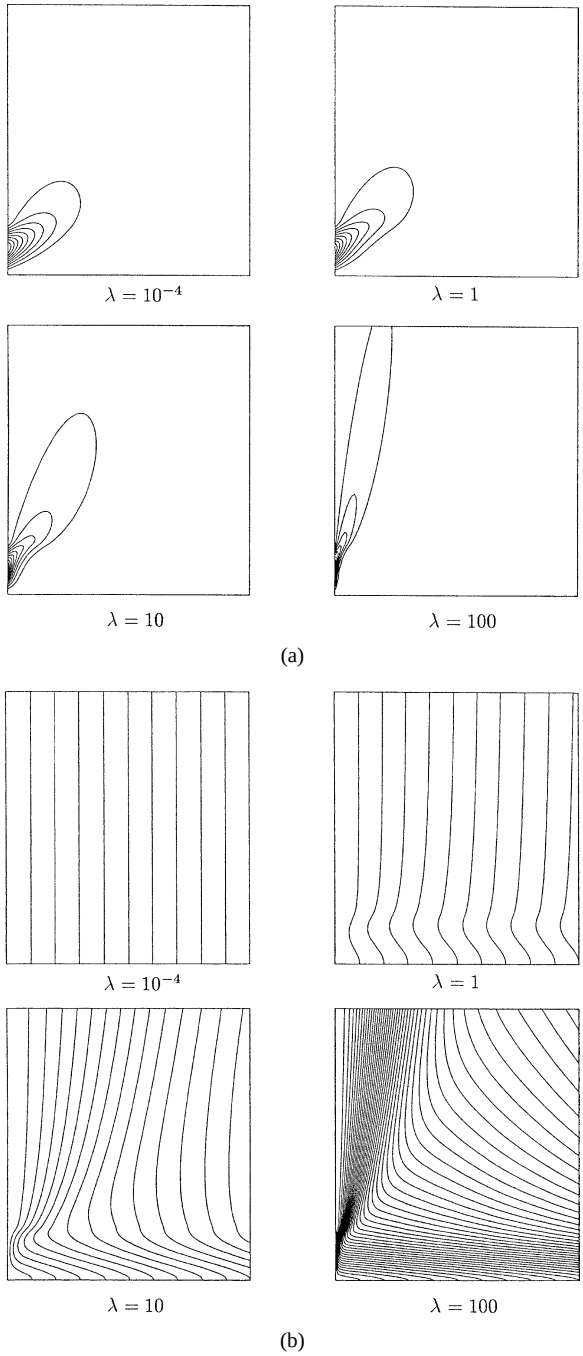

Fig. 12. (a) Isotherms and (b) streamlines for $P \to \infty$ for $\lambda = 10^{-4}$, 1, 10, and 100. 9 equally spaced isotherms are drawn at an interval of 0.1 and equally spaced streamlines are drawn at an interval of 1.0.

clearly display the increasing strength of the overall flow due to buoyancy forces as λ increases, as may be seen in Fig. 12(b).

5. Conclusions

In this paper the main features and results of a theoretical investigation of mixed convection flow in a narrow vertical duct filled with a porous medium where the boundaries are held at identical cold temperatures with the exception of local heating on one wall. Both analytical and numerical results are obtained for some values of the governing parameters P (or Pe) and λ. The isotherms and streamlines, as well as the heat transfer from both walls have been determined and presented as a function of these parameters and of x, the streamwise distance. Good agreement between the numerical and analytical results has been shown to exist. On the other hand, it was shown that the interaction between the heat transfer and the fully developed flow has a significant effect in situations where the parameters P and λ take limiting values. In particular, regions of reversed flow are obtained for $\lambda = 2.5$ and P small. We have found those values of λ, as a function of P, above which recirculating flow will occur. Approximate expressions (correlating equations) were obtained numerically for such critical values of λ for both small and large values of P.

It is not possible to compare the present results with those of Hadim [8] since the temperature profiles considered there are different from those in the present paper, and, further, Hadim's work lies squarely within the elliptic regime where upstream influence is significant, whereas the present work is within the parabolic regime due to the narrowness of the gap compared with the streamwise distance over which the boundary temperature profile varies. Likewise, we have not been able to compare with experimental results due to their absence within the open literature.

Acknowledgements

One of the authors (I.P.) gratefully acknowledges the support of this work by Alexander von Humboldt–Fellowship while he visited the Brandenburg Technical University of Cottbus, Germany. The authors also thank the anonymous referees who helped to improve the manuscript.

References

[1] D.B. Ingham, I. Pop (Eds.), Transport Phenomena in Porous Media, vol. 2, Pergamon, Oxford, 1998, 2002.
[2] D.A. Nield, A. Bejan, Convection in Porous Media, second ed., Springer, New York, 1999.
[3] K. Vafai (Ed.), Handbook of Porous Media, Dekker, New York, 2000.
[4] I. Pop, D.B. Ingham, Convective Heat Transfer: Mathematical and Computational Modelling of Viscous Fluids and Porous Media, Pergamon, Oxford, 2001.
[5] K. Vafai, H. Hadim, Overview of current computational studies of heat transfer in porous media and their applications—natural and mixed convection, in: W.J. Minkowycz, E.M. Sparrow (Eds.), Advanced Numerical Heat Transfer II, Taylor & Francis, New York, 2000, pp. 331–369.
[6] F.C. Lai, Mixed convection in saturated porous media, in: K. Vafai (Ed.), Handbook of Porous Media, Dekker, New York, 2000, pp. 605–661, Chapter 14.
[7] T. Mahmood, J.H. Merkin, Mixed convection flow in narrow vertical ducts, Wärme- und Stoffübertr. 24 (1989) 251–271.
[8] H.A. Hadim, Numerical study of non-Darcy mixed convection in a vertical porous channel, J. Thermophys. Heat Transfer 8 (1994) 371–373.
[9] H.A. Hadim, G. Chen, Non-Darcy mixed convection in a vertical porous channel with asymmetric wall heating, J. Thermophys. Heat Transfer 8 (1994) 805–808.
[10] F.C. Lai, V. Prasad, F.A. Kulacki, Aiding and opposing mixed convection in a vertical porous layer with the finite wall heat source, Int. J. Heat Mass Transfer 31 (1998) 1049–1061.
[11] T. Cebeci, P. Bradshaw, Physical and Computational Aspects of Convective Heat Transfer, Springer, New York, 1989.